JACS
JOURNAL OF THE AMERICAN CHEMICAL SOCIETY

Communication

pubs.acs.org/JACS

The Effect of a Widespread Cancer-Causing Mutation on the Inactive to Active Dynamics of the B-Raf Kinase

Kristen A. Marino, Ludovico Sutto, and Francesco Luigi Gervasio*

Department of Chemistry, University College London, London, U.K.

Supporting Information

ABSTRACT: Protein kinases play a key role in regulating cellular processes. Kinase dysfunction can lead to disease, making them an attractive target for drug design. The B-Raf kinase is a key target for the treatment of melanoma since a single mutation (V600E) is found in more than 50% of all malignant melanomas. Despite the importance of B-Raf in melanoma treatment, the molecular mechanism by which the mutation increases kinase activity remains elusive. Since kinases are tightly regulated by a conformational transition between an active and inactive state, which is difficult to capture experimentally, large-scale enhanced-sampling simulations are performed to examine the mechanism by which the V600E mutation enhances the activity of the B-Raf monomer. The results reveal that the mutation has a twofold effect. First, the mutation increases the barrier of the active to inactive transition trapping B-Raf in the active state. The mutation also increases the flexibility of the activation loop which might speed-up the rate-limiting step of phosphorylation. Both effects can be explained by the formation of salt-bridges with the Glu600 residue.

Kinase proteins play a key role in signaling pathways that control cellular processes such as cell growth, proliferation, and differentiation. Kinases catalyze phosphorylation, the transfer of a phosphate group from ATP to a substrate protein, which is necessary for regulating the activity of many enzymes in the cell, including many kinases themselves. The activity of kinases is regulated by a tightly controlled transition between an active state and a catalytically inactive state.

Dysfunction of kinases has been implicated in a number of diseases, most notably cancer. In many cases, the active−inactive equilibrium is shifted toward the active state leading to enhanced signaling and e.g. uncontrolled cell growth. Hence, kinases are important targets for the development of novel therapeutics to treat such diseases. One kinase implicated in cancer is B-Raf, which is part of the RAS-RAF-MEK-ERK signaling pathway. While there are three isoforms of Raf (A-Raf, B-Raf, and C-Raf), B-Raf is the most frequently mutated in human cancers. B-Raf is mutated in 66% of malignant melanomas, and a single point mutation, V600E, accounts for 80% of these B-Raf mutations.[1] (Due to an error in the early sequencing of the BRAF gene, some report this mutation as V599E.[2]) The V600E mutation is highly activating leading to a 500% increase in basal activity compared to wild-type (WT) B-Raf.[3] Thus, the B-Raf V600E mutant appears to be a promising target for the treatment of melanoma and currently two inhibitors targeting the mutant have been approved by the FDA.[4] One side effect of these treatments is the development of secondary tumorigenesis driven by an "inhibitor paradox", whereby a drug binding to one monomer transactivates a drug-free partner.[5] In the cell, WT Raf binds to activated Ras at the cell membrane where it is activated through dimerization and phosphorylation. The overactivated RAS will promote dimerization of Raf, and binding of an inhibitor to one Raf protomer transactivates the other.[5] Despite B-Raf being an important target for drug discovery, little is known about the mechanism by which the V600E mutation activates B-Raf and why the mutant does not require dimerization to be catalytically active.[6] A better understanding of the effects of this widespread mutation could open novel pathways in the development of inhibitors to overcome the paradoxical activation by, e.g., disrupting interactions which trap the mutant in its active state and/or favor dimerization.

The kinase family is characterized by a dual-lobe structure (Figure 1). The smaller N-lobe is made of a β-sheet and an α-helix (the αC-helix). Two of the β-strands are connected by a Gly-rich loop (P-loop) which is important for ATP orientation. The C-lobe is larger and mostly helical with the active site located in a cleft between the two lobes. The C-lobe contains an activation loop (A-loop) which has significantly different conformations in the active and inactive states. In the active state, the A-loop is open allowing for ATP and substrate binding while, in the inactive state, the A-loop is closed blocking the active site. Another feature of the C-lobe is a short α-helix, known as the αG-helix.

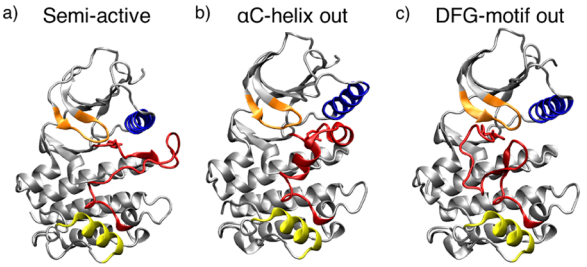

Figure 1. Crystal structures of the catalytic domain of B-Raf in the semiactive, αC-helix out, and DFG-motif out conformations. The missing loops were added with MODELER.[7] The important structural elements are colored: P-loop (orange), αC-helix (blue), A-loop (red), αG-helix (yellow). All structures were rendered with VMD.[8]

Received: February 9, 2015
Published: April 13, 2015

DOI: 10.1021/jacs.5b01421
J. Am. Chem. Soc. 2015, 137, 5280−5283

The first three residues of the A-loop, DFG, are highly conserved in kinases. Many kinases adopt a DFG-motif out inactive structure where the side chain of the Phe residue is flipped, occupying the ATP-binding site and the Asp points out of the active site breaking a key salt bridge between Asp594 and Lys483 (Figure 2a). Another class of inactive structures is

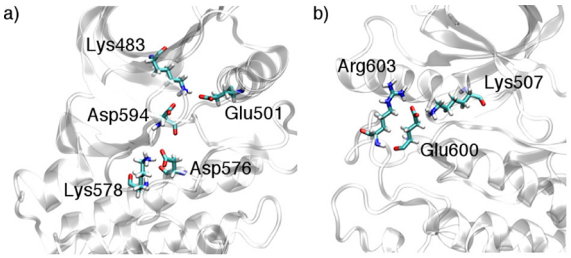

Figure 2. Key salt-bridge forming residues in (a) the active site of both WT and mutant B-Raf and (b) mutant B-Raf only.

characterized by the αC-helix shifted away from the N-lobe breaking another key salt bridge formed by Glu501 of the αC-helix with Lys483.

It has been postulated that the V600E mutation mimics phosphorylation since the two phosphorylation sites are at residues 599 and 602,[1] but crystal structures have been unable to confirm this. B-Raf has been crystallized in both inactive conformations, and in an open structure, typically called the active state but hereafter called the semiactive state for reasons to be discussed below. All of these crystal structures have been of the dimer with inhibitors bound except one.[9] While the crystal structures of WT and mutant B-Raf appear to be very similar, none of the mutant crystal structures has a fully resolved A-loop, which is where the V600E mutation is located. Thus, the crystal structures have been unable to provide a clear understanding of the effect of the mutation at the atomic level.

As the active−inactive transition is key to the regulation of kinases, and the crystal structure can only provide snapshots of the structure, a method examining the dynamics of the kinase is necessary. Computational approaches have been successfully applied to examine the effect of cancer-causing point mutations in several kinases.[10−14] The simulations of B-Raf available in the literature[15,16] are much too short to sample the significant conformational changes B-Raf undergoes when transitioning between the two states. Here we perform much longer MD simulations and use enhanced sampling methods, including the longest parallel tempering metadynamics (PT-metaD) sampling ever performed,[17] to reach the time scales on which the conformational changes take place. PTmetaD has been successfully applied to study the conformational changes in the Abl, Src, EGFR, and FGFR kinases.[13,14,18,19]

The WT semiactive, αC-helix out, and DFG-motif out B-Raf monomer structures of the kinase domain were taken as the best-resolved protomer in the dimer pdb structures of 4E26,[20] 3SKC,[21] and 4DBN,[22] respectively. The inhibitors in the pdb structures were removed, and the missing residues of the A-loop and the mutation were added using MODELLER.[7] Following system setup, the crystal structures were solvated and equilibrated according to the procedure described in the Supporting Information (SI). For all simulations, the AMBER99sb*-ildn force field[23] was used for the protein and the TIP3P model for the waters.[24]

For each of the six monomer structures, three WT and three mutant, two 500 ns molecular dynamics (MD) simulations were performed with the GROMACS 4.6.2 MD engine[25] to characterize the local dynamics of the six structures. Figure S5 shows these six structures colored by RMSF from one trajectory with the most flexible parts in blue and the least flexible in red. Comparing the WT structures, the αC-helix out inactive state is the least flexible. Surprisingly, the DFG-motif out inactive state appears to be the most flexible, especially in the αC-helix. The mutation does not have large effects on the flexibility, although it does explain some of the local differences. In the active state, the A-loop of the mutant is slightly less flexible due to the formation of a salt bridge between the side chains of Glu600 and Arg603 (Figure 2b). This salt-bridge remains formed for the entire duration of both trajectories in the semiactive state. While the presence of a Glu600-Arg603 salt-bridge has never been postulated to our knowledge, it has been suggested that formation of a salt-bridge between Glu600 and Lys507, the final residue of the αC-helix, has a stabilizing effect.[3] Here we find that the Glu600-Lys507 salt-bridge is not stable in one of the MD trajectories of the semiactive state and only transiently stable in the second trajectory.

The P-loop of the αC-helix out inactive state is more flexible in the mutant than the WT due to disruption of hydrophobic contacts between the N-lobe and A-loop. The Glu600-Arg603 salt-bridge remains intact for the entire length of the simulations, destabilizing the αC-helix out inactive state.

The MD results suggest that the V600E mutation stabilizes the active site and destabilizes the inactive state, agreeing with the experimental conclusions of Wan et al.,[3] but even at 500 ns, MD simulations are too short to capture significant conformational changes. Thus, we used PT-metaD simulations to characterize the active to inactive transition and calculate the corresponding free energy surfaces (FESs). PT-metaD simulations were performed with the PLUMED 1.3 plugin[26] for GROMACS to capture large scale conformational changes. Thirty-six replicas over a temperature range of 290−390 K were run for 1.9 μs for a total of 68.4 μs of sampling with exchanges attempted every 2 ps. The CVs used here are the distance from a reference state in terms of contact maps (see SI). Three CVs were used, each one referenced to one of the three states, the semiactive state (CV1), the αC-helix out inactive state (CV2), or the DFG-motif out inactive state (CV3). A similar combination of CVs has been successfully used together with PTmetaD to converge the conformational FES associated with the activation of the EGFR and FGFR kinases[13,14] and in many other complex biomolecular systems.[27]

The FESs of the WT and mutant B-Raf were constructed from the replica at 300 K after 1.9 μs of simulation time per replica. Figure 3 shows the free energy as a function of two of the CVs used for the PT-metaD. (Please see the SI, Figures S1 and S2, for a discussion of convergence.) A low value of the distance to the semiactive state indicates a conformation close to the semiactive state while a larger value indicates the conformation is far from the state. WT B-Raf sampled the semiactive state, αC-helix out inactive state, and a local minimum. The αC-helix out inactive state is 20 kJ/mol higher in energy than the semiactive state, and the free energy barrier for the inactive to semiactive transition is 10 kJ/mol while it is 40 kJ/mol for the semiactive to inactive transition. The energy barrier for the inactive to semiactive transition of the full enzyme in the cell is likely higher than 10 kJ/mol since our model only included the kinase domain. In the cell,

DOI: 10.1021/jacs.5b01421
J. Am. Chem. Soc. 2015, 137, 5280−5283

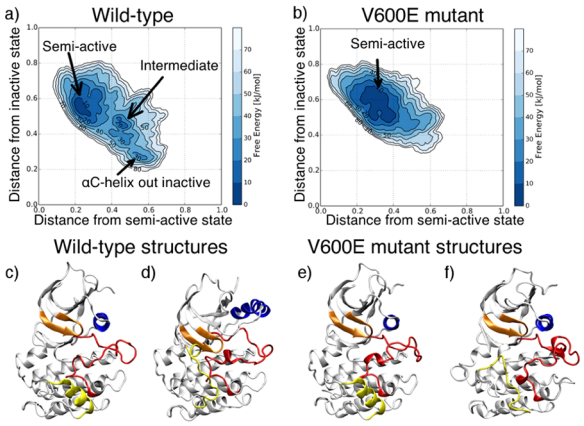

Figure 3. FES as a function of distance from semiactive state (x-axis) and distance from inactive state (y-axis) of the WT (a) and mutant (b) B-Raf. Structures represent (c) largest cluster in the WT semiactive state and (d) the possible intermediate structure in the WT active−inactive transition. For the mutant, (e,f) both structures are from clusters within the semiactive state.

the inactive state is stabilized by interactions between the kinase domain and its regulatory domains.[28]

The most striking difference between the FESs of the WT and mutant is that the αC-helix out inactive state located at CV2 0.2−0.3 has a much higher energy in the mutant B-Raf (Figures 3b and S4), suggesting that the mutant, in contrast to the WT, spends most of its time in the semiactive state. Indeed, when unbiased MD simulations of B-Raf V600E are started from the inactive state, they spontaneously relax to an intermediate conformation that represents a local free energy minimum (Figure S3). Also, the basin corresponding to the active state of the mutant (CV1 0.2−0.4) is much broader than the corresponding basin for the WT (CV1 0.2−0.3) suggesting that this state can adopt many more conformations in the mutant than in the WT. A further difference is noticed with respect to the stability of the αG helix as reported below.

To determine representative structures of the minima, clustering was performed on the 300 K replica to group the structures based on C_α rmsd. In the WT, the six clusters found in the semiactive minimum were very similar with respect to the structure and orientation of the N- and C-lobe. The most populated cluster is depicted in Figure 3c. The main difference between the clusters is in the conformation of the A-loop which is consistent with the inability to resolve the A-loop in crystal structures. In most active kinases, the A-loop is extended to allow access to the active site. Here, as previously reported in the case of EGFR,[13] none of the structures corresponding to the significantly populated clusters had a fully extended A-loop, and as a result, we refer to these structures as being in a semiactive state. Recent work by Haling et al. showed that the crystal structure of B-Raf in complex with its substrate MEK has a fully extended A-loop[29] suggesting that substrate binding and possibly phosphorylation may be required for the A-loop to be fully active. Active state kinases are characterized by other features seen in the semiactive structures, including the salt-bridges formed between the Asp of the DFG motif (Asp594) and Lys483 and between Glu501 in the αC-helix and Lys483 (Figure 2a), residues which are important for ATP binding in the active site. The active state also has a β-sheet formed by strands β6 and β9 held together by three H-bonds. All of the structures have at least two of the H-bonds formed. Two residues on the catalytic loop, Asp576 and Lys578, which are involved in coordination of ATP and the substrate protein in the active site form a salt-bridge in all of the semiactive structures.

A possible intermediate state for the active−inactive transition was found in the local minimum at a CV1 value of 0.5 and a CV2 value of 0.45 (Figure 3a,d). The αC-helix is shifted out similar to the αC-helix out inactive state, and the αG-helix is unfolded. Partial unfolding of the αG-helix at the transition state was also seen in a recent PT-metaD study of the EGFR kinase[13] suggesting that this unfolding may not be unique to B-Raf.

In the mutant, consistent with the large minimum seen for the semiactive state in the FES, the clusters correspond to a variety of structures which have very different A-loop configurations, two of which are seen in Figure 3e,f. In all ten structures corresponding to the most populated clusters, the mutated residue (E600) forms salt-bridges with Arg603 and/or Lys507. The salt-bridges formed by the E600 increase the stability of the β6/β9-sheet. The hitherto stabilized β-sheet has a dual effect. It increases the barrier to the inactive conformation while also enhancing the flexibility of the A-loop.

The barrier to adopt the inactive conformation is higher because, in order for the A-loop to fold to its inactive structure, the β6/β9-sheet needs to break. Another feature of some of the mutant cluster centers is an unfolded αG-helix, which is interesting because the intermediate structure identified for the WT has an unfolded αG-helix. Figure 4a,b shows the reweighted

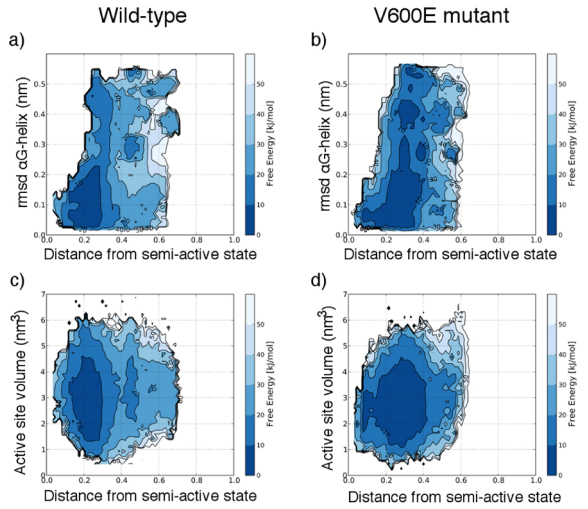

Figure 4. Reweighted FESs for (a,c) WT and (b,d) mutant B-Raf of the distance from the semiactive state (x-axis) and the rmsd of the αG-helix (a,c) or the volume of the ATP-binding site (b,d). The scale represents the energy relative to the minimum.

FES[30] of the rmsd of the αG helix with respect to an ideal α-helix on the x-axis and CV1 on the y-axis. As the value of the rmsd increases (and the αG-helix unfolds) the free energy barrier for the semiactive state is very low in the mutant. Interestingly, one of the WT clusters that is higher in energy than the semiactive state also had an unfolded αG-helix but maintains a formed β6/β9-sheet close to the start of the A-loop.

By lowering the energy penalty to break the hydrophobic contacts at the end of the A-loop, the salt-bridges formed by E600 also increase the flexibility of the A-loop, which in turn leads to a larger ATP binding cavity. The volume of the ATP-binding site was estimated using mdpocket[31] and is plotted as a function of CV1, the distance from the semiactive state (Figure

DOI: 10.1021/jacs.5b01421
J. Am. Chem. Soc. 2015, 137, 5280−5283

4c,d). This set of FESs was obtained by using the reweighting technique of Tiwary and Parrinello.[30] The great diversity of semiactive A-loop conformations in the mutant, and a larger cavity should enhance the ability to release the products of the phosphorylation. Since the slowest step in the phosphorylation cycle corresponds in most kinases to product release,[32] a more flexible cavity, having on average a larger volume, could lead to higher turnover of B-Raf and hence a faster rate of phosphorylation.

In conclusion, the increased activity of the V600E mutant is twofold: increased flexibility of the A-loop which likely promotes the release of the products following phosphorylation of the substrate and an increased energy barrier between the active and inactive state. Both are due to salt-bridges formed by Glu600 with Arg603 and Lys507. While the importance of the Glu600-Lys507 salt-bridge has been recognized, the formation of the Glu600-Arg603 salt-bridge as a stabilizing element has not been promoted. Disrupting the formation of the Glu600-Arg603 salt-bridge could be a viable pathway for inhibitor development. A possible intermediate in the active to inactive transition of WT B-Raf has also been identified. An inhibitor that targets this state may be a viable option for cancers with Ras mutations. The intermediate and minimum energy structures have also revealed the importance of the αG-helix in the conformational changes in B-Raf, which may be applicable to other kinases. Since WT and mutant B-Raf have very similar backbone structures and the resolution of the A-loop in crystal structures is very poor, our simulations have revealed new insight into the structure and dynamics of the B-Raf kinase.

■ ASSOCIATED CONTENT

Supporting Information

Further computational details and figures. This material is available free of charge via the Internet at http://pubs.acs.org.

■ AUTHOR INFORMATION

Corresponding Author

*f.l.gervasio@ucl.ac.uk

Notes

The authors declare no competing financial interest.

■ ACKNOWLEDGMENTS

This work was supported by the People Programme (Marie Curie Actions, FP7/2007-2013) under REA Grant Agreement No. 299136 and in part by the Engineering and Physical Sciences Research Council [Grant No. EP/M013898/1]. We thank PRACE Research Infrastructure resources MareNostrum and Curie (FP7 RI-283493), PRACE-3IP project (FP7 RI-312763) resources Sisu and Taito at the CSC in Finland, and the HECBioSim resource Archer in the U.K. Thanks to Dr. G. Saladino for many helpful discussions.

■ REFERENCES

(1) Davies, H.; et al. *Nature* **2002**, *417*, 949.
(2) Wellbrock, C.; Karasarides, M.; Marais, R. *Nat. Rev. Mol. Cell Biol.* **2004**, *5*, 875.
(3) Wan, P. T. C.; Garnett, M. J.; Roe, S. M.; Lee, S.; Niculescu-Duvaz, D.; Good, V. M.; Jones, C. M.; Marshall, C. J.; Springer, C. J.; Barford, D.; Marais, R. *Cell* **2004**, *116*, 855.
(4) Holderfield, M.; Deuker, M. M.; McCormick, F.; McMahon, M. *Nat. Rev. Cancer* **2014**, *14*, 455.
(5) Poulikakos, P. I.; Rosen, N. *Cancer Cell* **2011**, *19*, 11.
(6) Röring, M.; Herr, R.; Fiala, G. J.; Heilmann, K.; Braun, S.; Eisenhardt, A. E.; Halbach, S.; Capper, D.; von Deimling, A.; Schamel, W. W.; Saunders, D. N.; Brummer, T. *EMBO J.* **2012**, *31*, 2629.
(7) Sali, A.; Blundell, T. L. *J. Mol. Biol.* **1993**, *234*, 779.
(8) Humphrey, W.; Dalke, A.; Schulten, K. *J. Mol. Graphics* **1996**, *14*, 33.
(9) Thevakumaran, N.; Lavoie, H.; Critton, D. A.; Tebben, A.; Marinier, A.; Sicheri, F.; Therrien, M. *Nat. Struct. Mol. Biol.* **2015**, *22*, 37.
(10) Gkeka, P.; Evangelidis, T.; Pavlaki, M.; Lazani, V.; Christoforidis, S.; Agianian, B.; Cournia, Z. *PLoS Comput. Biol.* **2014**, *10*, e1003895.
(11) Gibbons, D. L.; Pricl, S.; Posocco, P.; Laurini, E.; Fermeglia, M.; Sun, H.; Talpaz, M.; Donato, N.; Quintás-Cardama, A. *Proc. Natl. Acad. Sci. U.S.A.* **2014**, *111*, 3550.
(12) Doss, G. P.; Rajith, B.; Chakraborty, C.; NagaSundaram, N.; Ali, S. K.; Zhu, H. *Sci. Rep.* **2014**, *4*, 5868.
(13) Sutto, L.; Gervasio, F. L. *Proc. Natl. Acad. Sci. U.S.A* **2013**, *110*, 10616.
(14) Bunney, T. D.; Wan, S.; Thiyagarajan, N.; Sutto, L.; Williams, S. V.; Ashford, P.; Koss, H.; Knowles, M. A.; Gervasio, F. L.; Coveney, P. V.; Katan, M. *EBioMedicine* **2015**, *2*, 194−204.
(15) Fratev, F. F.; Jónsdóttir, S. O. *BMC Struct. Biol.* **2009**, *9*, 47.
(16) Fratev, F.; Jónsdóttir, S. O.; Mihaylova, E.; Pajeva, I. *Mol. Pharmaceutics* **2009**, *6*, 144.
(17) Bussi, G.; Gervasio, F. L.; Laio, A.; Parrinello, M. *J. Am. Chem. Soc.* **2006**, *128*, 13435.
(18) Lovera, S.; Sutto, L.; Boubeva, R.; Scapozza, L.; Dölker, N.; Gervasio, F. L. *J. Am. Chem. Soc.* **2012**, *134*, 2496.
(19) Dölker, N.; Górna, M. W.; Sutto, L.; Torralba, A. S.; Superti-Furga, G.; Gervasio, F. L. *PLoS Comput. Biol.* **2014**, *10*, e1003863.
(20) Qin, J.; Xie, P.; Ventocilla, C.; Zhou, G.; Vultur, A.; Chen, Q.; Liu, Q.; Herlyn, M.; Winkler, J.; Marmorstein, R. *J. Med. Chem.* **2012**, *55*, 5220.
(21) Wenglowsky, S.; et al. *Bioorg. Med. Chem. Lett.* **2011**, *21*, 5533.
(22) Okaniwa, M.; et al. *J. Med. Chem.* **2012**, *55*, 3452.
(23) Lindorff-Larsen, K.; Piana, S.; Palmo, K.; Maragakis, P.; Klepeis, J. L.; Dror, R. O.; Shaw, D. E. *Proteins: Struct., Funct., Bioinf.* **2010**, *78*, 1950.
(24) Jorgensen, W. L.; Chandrasekhar, J.; Madura, J. D.; Impey, R. W.; Klein, M. L. *J. Chem. Phys.* **1983**, *79*, 926.
(25) Hess, B.; Kutzner, C.; Spoel, D. V. D.; Lindahl, E. *J. Chem. Theory Comput.* **2008**, *4*, 435.
(26) Bonomi, M.; Branduardi, D.; Bussi, G.; Camilloni, C.; Provasi, D.; Raiteri, P.; Donadio, D.; Marinelli, F.; Pietrucci, F.; Broglia, R. A.; Parrinello, M. *Comput. Phys. Commun.* **2009**, *180*, 1961−1972.
(27) Cavalli, A.; Spitaleri, A.; Saladino, G.; Gervasio, F. L. *Acc. Chem. Res.* **2015**, *48*, 277−285.
(28) Udell, C. M.; Rajakulendran, T.; Sicheri, F.; Therrien, M. *Cell. Mol. Life Sci.* **2011**, *68*, 553.
(29) Haling, J.; Sudhamsu, J.; Yen, I.; Sideris, S.; Sandoval, W.; Phung, W.; Bravo, B.; Giannetti, A.; Peck, A.; Masselot, A.; Morales, T.; Smith, D.; Brandhuber, B.; Hymowitz, S.; Malek, S. *Cancer Cell* **2014**, *26*, 402.
(30) Tiwary, P.; Parrinello, M. *J. Phys. Chem. B* **2014**, *119*, 736.
(31) Schmidtke, P.; Le Guilloux, V.; Maupetit, J.; Tufféry, P. *Nucleic Acids Res.* **2010**, *38*, 582.
(32) Adams, J. A. *Chem. Rev.* **2001**, *101*, 2271.

DOI: 10.1021/jacs.5b01421
J. Am. Chem. Soc. 2015, 137, 5280−5283